INVERSE ANALYSIS OF HORIZONTAL EARTH STRESSES BASED ON BOREHOLE MECHANICS AND SOFT COMPUTING

Shike Zhang*, Shunde Yin**

This paper presents a hybrid model based on the displacement back analysis to estimate the earth stress magnitude and direction from the obtained borehole displacements. An artificial neural network (ANN) is used to map the non-linear relationship between the maximum horizontal earth stress, σ_{H}, the minimum horizontal earth stress, σ_{h}, the direction of the largest horizontal earth stress, θ and the borehole displacements. The genetic algorithm (GA) is used to search the set of unknown earth stresses and direction according to the objective function. Results of the numerical experiments show that the displacement back analysis method can effectively identify the earth stress based on the wellbore motions during drilling.

Keywords: *earth stress, borehole mechanics, inverse analysis, artificial neural network, genetic algorithm*

1. Introduction

Earth stress is the original stress field in the rock formation without any engineering disturbances. Earth stress plays a vital role in securing wellbore stability and optimizing well stimulation operations. Thus, it is necessary to have the knowledge of earth stress in order to perform any rock stress analysis and failure evaluation.

Generally, there are two approaches to estimate the earth stress in rock engineering, the direct approach and the indirect approach [6, 20]. In the direct approach, the magnitude and orientation of the horizontal earth stress can be directly determined by using the testing techniques, such as hydraulic fracturing test or overcoring gauge test. It was reported that the hydraulic fracturing method is less accurate in estimating the maximum horizontal stress, and the overcoring method is mainly suitable for depth down to 1000 m [8, 13, 18, 20, 31].

In the indirect approach, the magnitude and orientation of the horizontal earth stress can be mainly obtained through borehole breakout, acoustic emission, fault plane solution, differential strain analysis, inelastic strain relaxation, core discing, observation of discontinuity states and inverse analysis [1, 2, 4, 10, 11, 12, 14, 26]. The previous inverse analysis as an indirect approach is mostly based on the linear elastic theory, which could lead to the error in estimation of the largest and smallest horizontal earth stresses and their direction [3, 24].

The objective of this work is to investigate the largest and smallest horizontal earth stresses and the azimuth of the maximum horizontal earth stress for the fractured rock

* S.Zhang, Ph.D., School of Civil Engineering and Architecture, Anyang Normal University, Anyang, Henan, 455000, China

** S. Yin, Ph.D., Department of Chemical & Petroleum Engineering, University of Wyoming, Laramie, WY, 82071, USA

formation based on the borehole displacements during drilling. For borehole stability analysis of fractured formation, a large number of methods considering fractures in solids are available, for example, three-dimensional numerical manifold method [15], smooth particle hydrodynamic mehtod [29], free hexagon method [28], and discrete element method [33]. The borehole displacements can be easily obtained through the caliper logs and ultrasonic borehole televiewer [16, 22, 27, 32]. In this work, we use the displacement based inverse analysis method and consider the more realistic behavior of the rock mass. Firstly, an artificial neural network (ANN) is applied to map a non-linear relationship between the assumed earth stress and the borehole displacements from a coupled geomechanics model. The distinct element method (UDEC) [9, 19] is used in this paper to create the training and testing samples for ANN. Next, a robust objective (error) function is established based on the non-linear relationship. Finally, a genetic algorithm (GA) is chosen in this study to search the set of unknown earth stresses and direction according to the objective function. Lastly, numerical experiments are conducted to verify the hybrid model based on the displacement back analysis.

2. Thermoporoelastoplasticity and Distinct Element Method (DEM)

Drilling process involves strong coupling among heat transfer, fluid flow, and rock mass deformation. Universal Distinct Element Code (UDEC) [19] is a numerical modeling code for advanced geotechnical analysis of soil, rock, and structural support in two dimensions. UDEC is usually used to simulate the response of discontinuous media (such as jointed rock) that is subject to either static or dynamic loading, and allows explicit of blocks of rock and how they interact with each other. There are three main types of contacts, the corner-to-corne, corner-to-edge, and edge-to-edge, the detailed description can be found in reference [36]. The fracture conductivity is dependent on the aperture of the contact. The deformation of a discontinuous rock formation is comprised of deformation of the intact rock blocks and the rock discontinuities. The material model of deformation block uses plasticity model of Drucker-Prager in a thermoporoelastoplasticity framework; and the material model of fractured rock adopts fractures contact which follow the coulomb slid model in the numerical model of discrete element. Therefore, UDEC designed for discontinuous media has the capability to conduct the coupled thermal-hydraulic-mechanical (THM) analysis in this paper.

2.1. Constitutive model

The constitutive model is the incremental numerical algorithm, it can be expressed as [20]

$$\mathrm{d}\sigma' = \mathbf{D}^{\mathrm{ep}}(\mathrm{d}\varepsilon - \mathrm{d}\varepsilon^{\mathrm{p}}) - \frac{18\,K\,G}{3\,K + 4\,G}\,\beta\,\mathrm{d}T + \alpha\,\mathrm{d}p \tag{1}$$

where $\mathrm{d}\sigma'$ is the effective stress increment; $\mathrm{d}\varepsilon$ is the total strain increment; $\mathrm{d}\varepsilon^{\mathrm{p}}$ is the plastic strain increment; K is the bulk modulus; G is shear modulus; β is the linear thermal expansion coefficient; $\mathrm{d}T$ is the temperature increment; α is the Biot's coefficient; $\mathrm{d}p$ is the pore pressure increment. Moreover, $\mathbf{D}^{\mathrm{ep}}$ is the elastoplastic stress-strain matrix, which can be written as

$$\mathbf{D}^{\mathrm{ep}} = \mathbf{D}^{\mathrm{e}} - \frac{\mathbf{D}^{\mathrm{e}} \dfrac{\partial Q}{\partial \sigma'} \left\{ \dfrac{\partial F}{\partial \sigma'} \right\}^{\mathrm{T}} \mathbf{D}^{\mathrm{e}}}{-\dfrac{\partial F}{\partial \kappa} \left\{ \dfrac{\partial F}{\partial \varepsilon^{\mathrm{p}}} \right\}^{\mathrm{T}} \dfrac{\partial Q}{\partial \sigma'} + \left\{ \dfrac{\partial F}{\partial \sigma'} \right\}^{\mathrm{T}} \mathbf{D}^{\mathrm{e}} \dfrac{\partial Q}{\partial \sigma'}} \,, \tag{2}$$

$$\mathbf{D}^{\mathrm{e}} = \frac{E}{(1+\nu)(1-2\nu)} \begin{bmatrix} 1-\nu & \nu & 0 \\ \nu & 1-\nu & 0 \\ 0 & 0 & \dfrac{1-2\nu}{2} \end{bmatrix} . \tag{3}$$

In these equations, E is Young's modulus, ν is Poisson's ratio, κ is the hardening parameter. F is the yield function, and Q is the plastic potential function.

For linear Drucker-Prager yield criteria, the yield function F is given as

$$F = q_\varphi \, I_1 + \sqrt{J_2} - H_\varphi \,, \tag{4}$$

$$I_1 = \frac{1}{3} (\sigma_1' + \sigma_2' + \sigma_3') \,, \tag{5}$$

$$J_2 = \frac{1}{6} [(\sigma_1' - \sigma_2')^2 + (\sigma_2' - \sigma_3')^2 + (\sigma_3' - \sigma_1')^2] + {\sigma_{12}'}^2 \,, \tag{6}$$

$$q_\varphi = \frac{6}{\sqrt{3}\,(3 + \sin\varphi)} \sin\varphi \,, \tag{7}$$

$$H_\varphi = \frac{6}{\sqrt{3}\,(3 + \sin\varphi)} \, c \cos\varphi \tag{8}$$

where I_1 is the mean normal effective stress, J_2 is the deviatoric effective stress, $\sigma_1', \sigma_2', \sigma_3'$ are the three effective normal stresses, σ_{12}' is the effective tangential stress, φ is the friction angle, c is the cohesion.

A non-associated flow rule is employed to simulate the dilatant behavior of rock, the plastic potential function Q can be expressed as

$$Q = q_\psi \, I_1 + \sqrt{J_2} \tag{9}$$

where ψ is the dilation angle.

2.2. Mud infiltration model

The mean velocity for laminar viscous flow between parallel plates can be expressed as

$$V = k_{\mathrm{f}} \, B \tag{10}$$

in which V is the mean velocity, B is the hydraulic gradient, and the facture hydraulic conductivity is given by

$$k_{\mathrm{f}} = k_{\mathrm{j}} \, a^2 \, g \tag{11}$$

where k_{j} is the joint permeability factor, a is the contact hydraulic aperture, g is the acceleration of gravity.

Thus, the flow rate per unit width can be written as

$$q = -k_{\mathrm{j}} \, a^3 \, \frac{\mathrm{d}p}{l} \tag{12}$$

where dp is pore pressure difference between adjacent domains, l is the length assigned to the contact between the domains.

It can be seen that the facture aperture dominates the extent of mud infiltration into the fracture under the same stress condition.

2.3. Heat transfer equation

The basic equation of conductive heat transfer is Fourier's law [5], which can be written as

$$Q_i = -k_{ij} \frac{\partial T}{\partial x_j} \tag{13}$$

where Q_i is flux in the i-direction, k_{ij} is thermal conductivity tensor, T is temperature.

Also, for any mass, the change in temperature can be expressed as

$$\frac{\partial T}{\partial t} = \frac{1}{C_{\mathrm{p}}\, \varrho} \left[\frac{\partial Q_{\mathrm{x}}}{\partial x} + \frac{\partial Q_{\mathrm{y}}}{\partial y} \right] \tag{14}$$

where Q_{x} and Q_{y} are net heat flow into mass in x-direction and y-direction, respectively, C_{p} is the specific heat, ϱ is mass density.

3. Displacement back analysis by artificial neural network and genetic algorithm

3.1. Artificial neural network

The artificial neural network (ANN) was originally developed in the1940s by McCulloch and Pitts [23]. An ANN is an information processing paradigm that is inspired by the way biological nervous systems, such as the brain, process information. The key element of this paradigm is the novel structure of the information processing system. An ANN consists of a great number of nodes and weights between nodes. Except for the input nodes, each node is a processing element (or neuron) with a nonlinear activation function. Network output changes according to difference of connected type, weight and activation function. Network itself is a type of natural algorithm or logical expression. Therefore, neural networks can be considered to be non-linear statistical data modeling tools. They are usually applied to model complex non-linear relationships between inputs and outputs, or to find patterns in data. Neural networks are used as components in larger systems that combine both adaptive and non-adaptive elements, while the adaptive system is more suitable for real-world problem solving. Therefore, in most cases an ANN is an adaptive system that changes its structure based on external or internal information that flows through the network during the learning phase. A single artificial neuron with a node threshold b, connection weights w_i $(i = 1, 2, \ldots, n)$ and a transfer function $y^{(j)} = f(u^{(j)})$ is shown in Fig. 1. For each pattern j $(j = 1, 2, \ldots, p)$, all patterns can be expressed in matrix notation as [25]

$$\begin{bmatrix} u^{(1)} \\ u^{(2)} \\ \vdots \\ u^{(p)} \end{bmatrix} = \begin{bmatrix} x_1^{(1)} & x_2^{(1)} & \cdots & x_n^{(1)} & 1 \\ x_1^{(2)} & x_2^{(2)} & \cdots & x_n^{(2)} & 1 \\ \vdots & \vdots & \ddots & \vdots & \vdots \\ x_1^{(p)} & x_2^{(p)} & \cdots & x_n^{(p)} & 1 \end{bmatrix} \begin{bmatrix} w_1 \\ w_2 \\ \vdots \\ w_n \\ b \end{bmatrix} \tag{15}$$

or in a more compact form,

$$u^{(i)} = x_1^{(i)}\, w_1 + x_2^{(i)}\, w_2 + \cdots + x_n^{(i)}\, w_n + b \qquad \text{for} \quad i = 1, 2, \ldots, p\ .$$

ANN is used in this paper to represent the non-linear relationship between the maximum and minimum horizontal earth stresses, the azimuth of the maximum horizontal earth stress and the borehole displacements. This is essentially a mathematical model defining a function $\mathrm{ANN}(X)$:

$$\begin{aligned} \mathrm{ANN}(X) &: X \to Y \\ Y &= \mathrm{ANN}(X) \\ X &= (x_1, x_2, \ldots, x_n) \ , \\ Y &= (y^{(1)}, y^{(2)}, \ldots, y^{(p)}) \ . \end{aligned} \tag{16}$$

In this mathematical model, x_i $(i = 1, 2, \ldots, n)$ is the earth stress magnitude and direction, such as the maximum horizontal principal stress, σ_{H}, the minimum horizontal principal stress, σ_{h}, the azimuth of the largest horizontal principal stress, θ; $y(j)$ $(j = 1, 2, \ldots, p)$ is the borehole movements, such as the x-direction displacements u_{x} and the y-direction displacements u_{y}.

In order to establish the mathematical model $\mathrm{ANN}(X)$, it is needed to create displacement vectors corresponding to the given set of tentative earth stresses by using the numerical analysis method (e.g., UDEC). And then the ANN model is trained and tested with the tentative earth stresses as input and the created displacement vectors as output. The trained ANN is defined as the mathematical model $\mathrm{ANN}(X)$ (see Fig. 2).

The model ($\mathrm{ANN}(X)$) performance is able to be evaluated by mean square error (MSE) and correlation coefficient (R-value) [30]. MSE is given by eq. (17).

$$\mathrm{MSE} = \frac{1}{n} \sum_{i=1}^{n} (Y_i' - Y_i)^2 \tag{17}$$

where n is the number of samples, Y_i' and Y_i are the targets and the predicted values for $i = 1, 2, \ldots, n$, respectively.

Correlation coefficient (R-value) can be described by eq. (18).

$$R = \frac{\sum_{i=1}^{n} t_i \, p_i}{\sqrt{\sum_{i=1}^{n} t_i^2} \sqrt{\sum_{i=1}^{n} p_i^2}} \tag{18}$$

where n is the number of samples; $t_i = T_i - \dot{T}$, $p_i = P_i - \dot{P}$; T_i and $\dot{T}$ are the targets and the mean values of the target, respectively; P_i and $\dot{P}$ are the predicted values and the mean values of the predicted data set, respectively, $i = 1, 2, \ldots, n$.

Once the performance of the model ($\mathrm{ANN}(X)$) is satisfactory, it will be used to represent the non-linear relationship between input data and output data. And then the error function would be established for GA based on the non-linear relationship.

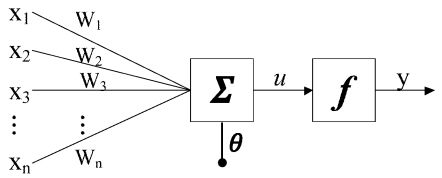

Fig.1: Schematic of a single artificial neuron

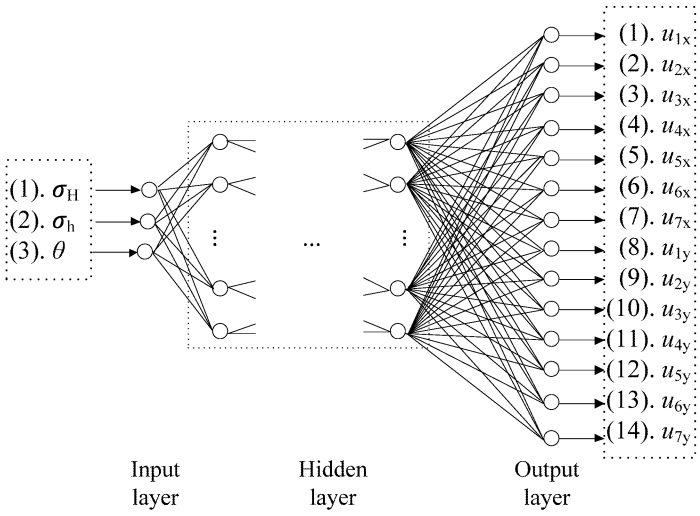

Fig.2: The neural network model

3.2. Genetic algorithm

The genetic algorithm (GA) was originally introduced in the early 1960s by John Holland [17]. GA is a global search and optimization technique based on the mechanism of natural selection and natural genetics. The technique starts with a set of solutions to the problem, this set of solutions is called the population, and each individual in the population is called a chromosome. The better the fitness of individual is, the more possibly the individual is to be selected. A roulette wheel selection is adopted to implement the selection operator of GA to determine which chromosomes are selected as parents. And parents create the next generations, new chromosomes, also called offspring through the crossover and mutation operations. Now the $X_i = [x_{i1}, x_{i2}, \ldots, x_{iN}]$ is used to represent chromosome i in the population $i = 1, 2, \ldots, pop\_size$. The fitness is $\text{eval}(X_i) = f(x)$ for each chromosome X_i, then total fitness can be calculated for the population by eq. (19):

$$S = \sum_{i=1}^{pop\_size} \text{eval}(X_i) \ . \tag{19}$$

The probability of being selected for each chromosome X_i is:

$$P_i = \frac{\text{eval}\, X_i}{S} \ . \tag{20}$$

As in any traditional approaches for displacement back analysis, an objective function is imperative to be defined when genetic algorithm is adopted to search the earth stresses and direction in a large search space. The objective function can be defined as

$$\text{fittness} = \min\left(\frac{1}{n}\sum_{i=1}^{n} |\,\text{ANN}_i(X) - U_i|\right) \tag{21}$$

where n represents displacement evaluation factors, $\text{ANN}_i(X)$ is the predicted displacement of the i^{th} evaluation factor. U_i is the monitored displacement of the i^{th} evaluation factor.

3.3. ANN-GA combination

For a hybrid ANN-GA model, results of back analysis can be assessed by the difference between the predicted displacements and the measured displacements. The entire flowchart of the hybrid ANN-GA back analysis method is illustrated in Fig. 3. The procedures can be described as follows [34, 35, 36] :

- *Step* 1 : Build proper ANN by determining initially network type and its algorithm, the number of hidden layers, number of hidden nodes and transfer functions.
- *Step* 2 : Initialize the weights and biases of the network.
- *Step* 3 : Train the initial network. The training process requires a set of examples of proper network behavior – network inputs and target outputs. The weights and bias of the network are iteratively adjusted during training.
- *Step* 4 : If the mean square error (MSE) between the network outputs and the target outputs is satisfied, or the epoch is reached, the training process will be stopped. Otherwise, repeat *Step* 3.
- *Step* 5 : Check the established artificial neural network model in terms of the network error performance and the data regression results.
- *Step* 6 : If both the network error performance and the data regression results are satisfied, the training will end. And then the best network model topology is obtained for genetic algorithm. Otherwise, go to *Step* 1.
- *Step* 7 : The initializations of GA parameter set including population size pop_size, the maximum generation max_gen, crossover probability P_{c}, mutation probability P_{m}, and the range of search space for parameters. In this study, in order to have an effective implementation of the GA, the real number encoding method is employed.
- *Step* 8 : Generate candidate individuals within the given range of parameters. And then the initial population is generated based on these candidate individuals. Here each chromosome (individual) represents an initial solution.
- *Step* 9 : Input the generated candidate solutions into the trained and tested neural network model ANN(X) from *Step* 6, and obtain the displacement values at given monitoring points.
- *Step* 10 : Use Eq. (21) to evaluate the fitness of the current individuals, i.e., the reasonability of the parameters set.
- *Step* 11 : If all individuals are evaluated, it will trace the best chromosome and go to *Step* 12. Otherwise, it will go to *Step* 9.
- *Step* 12 : If the given evolutionary generation is reached, or the best individuals (the properties of back identification), also the best chromosome, are obtained, then the algorithm terminates and outputs the earth stress magnitude and direction. Otherwise, go to *Step* 13.
- *Step* 13 : Execute the genetic operations, including selection, crossover and mutation. The next generations of the selected individuals are generated based on the genetic operations.
- *Step* 14 : Repeat Step 13 until all pop_size new individuals are generated. They are applied as new individuals (offspring).
- *Step* 15 : Using the generation of the best parent's individual to replace randomly an individual in the offspring.
- *Step* 16 : Take the offspring as parent and go to *Step* 9.

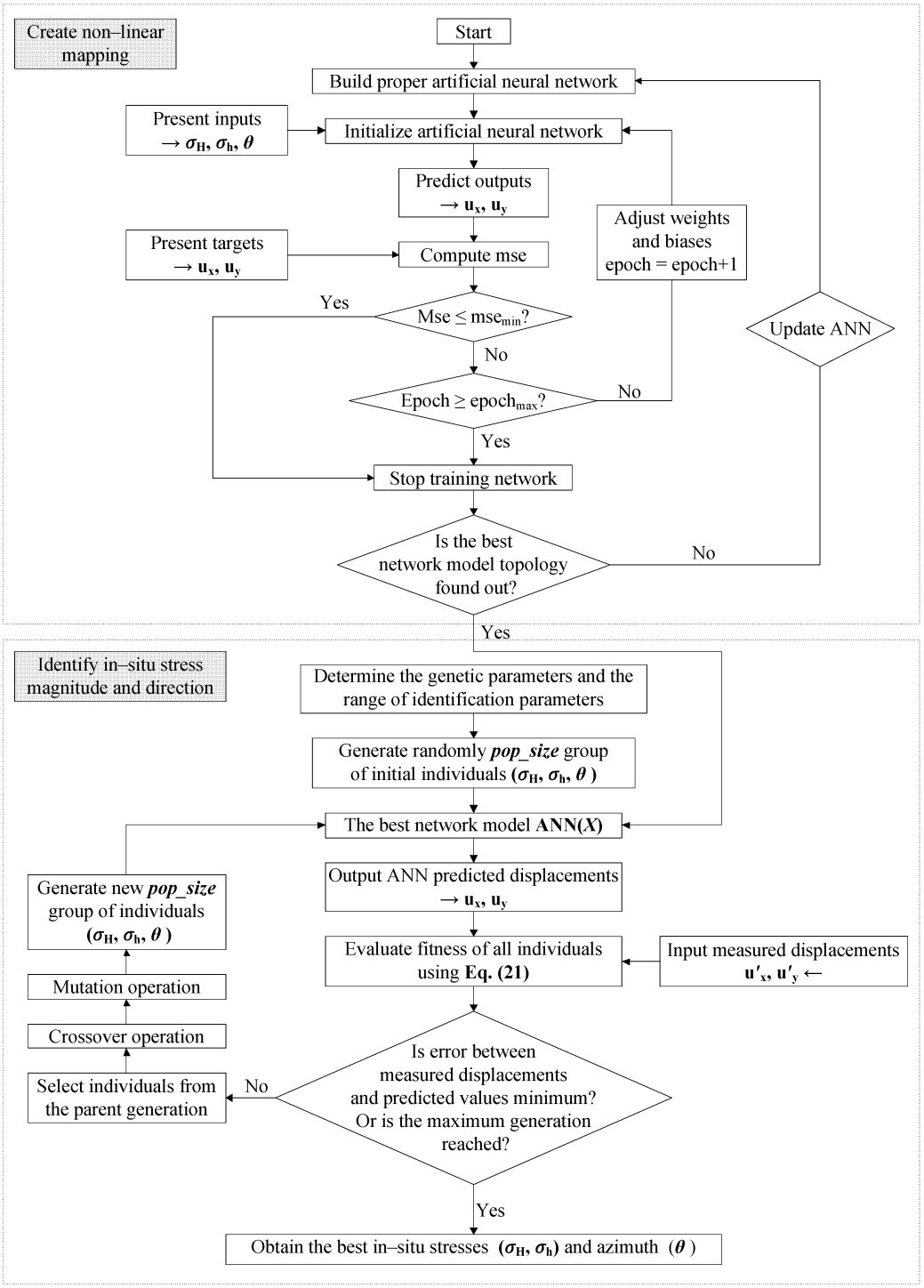

Fig.3: Flowchart of the hybrid ANN-GA

4. Numerical experiments on earth stress determination by displacement back analysis

4.1. Creation of training and testing samples

In order to provide valid inputs and outputs for artificial neural network, UDEC is used in this section to create the necessary data source. As can be seen from Fig. 4 the problem domain of the UDEC model corresponds to a two-dimensional horizontal square section, normal to the vertical borehole axis. The square section is 3×3 m with a borehole of 0.3 m in diameter, drilled at the center. The domain of mud infiltration is circular around the wellbore with a radius of $r = 0.2$ m. The azimuth of the maximum earth stress is defined in the east-north direction (EN). In this study, the Voronoi generator was used to create arbitrary size polygonal blocks that represents the rock mass. The three cracks are generated by using the joint generator, which is useful to simulate crack propagation. Seven fixed measured locations on the half wellbore wall are selected in each case to monitor the borehole deformations (e.g., x- and y-direction displacements). Figs. 5 and 6 show the fracture patterns and the monitored point locations.

The problem domain is located at a depth of 2000 m and is subjected to the largest and smallest horizontal earth stresses, σ_{H} and σ_{h}. The earth vertical stress (out-of-plane) is at a constant of $\sigma_{\mathrm{v}} = 43.16$ MPa, the problem domain is initially at the uniform pore pressure of $P_{\mathrm{o}} = 21$ MPa and at the uniform temperature of $T_{\mathrm{o}} = 100\,^{\circ}$C. After drilling the borehole domain is at the constant pore pressure of $P_{\mathrm{w}} = 26$ MPa and at the constant temperature

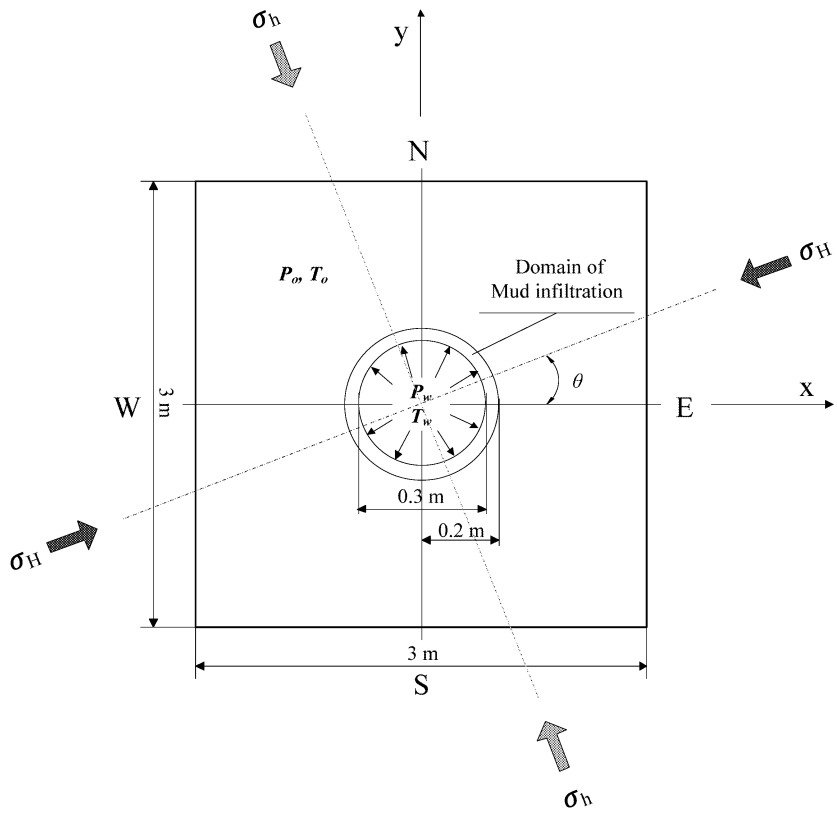

Fig.4: Borehole geometry and the problem domain

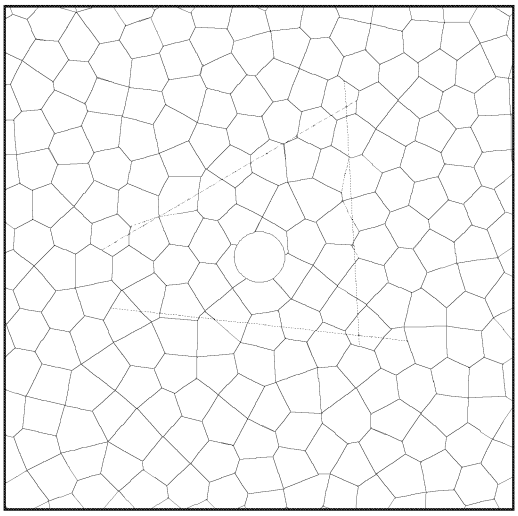

Fig.5: Fracture distribution in UDEC model

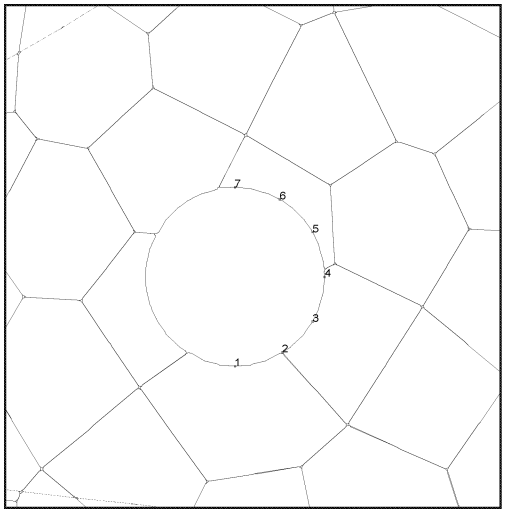

Fig.6: Measured locations on the half wellbore wall

Properties	Value
Intact rock	
Density (kg/m^3)	2278
Bulk modulus (GPa)	18.87
Shear modulus (GPa)	7.72
Friction angle (°)	36.2
Cohesion (MPa)	6.3
Dilation angle (°)	10
Tensile strength (MPa)	2.07
Fracture	
Normal stiffness (Pa/m)	90×10^{-10}
Shear stiffness (Pa/m)	60×10^{-10}
Friction angle (°)	36
Friction angle after mud infiltration (°)	25
Fracture permeability factor (1/(Pa s))	83.3
Residual aperture (m)	1.25×10^{-4}
Zero normal stress aperture (m)	2.5×10^{-4}
Tension limit (MPa)	0

Tab.1: Physical and mechanical properties of intact rock and fracture for numerical analysis [7]

Mud			Thermal parameters		
Density (kg/m^3)	Bulk modulus (GPa)	Cohesion (Pa)	Specific heat C_p (J/kg °C)	Expansion coefficient κ (10^{-6}/°C)	Conductivity k (W/m °C)
1200	0.1	0.1	890	5.2	4.0

Tab.2: Mud and thermal properties in numerical analysis

	Earth stresses and azimuth			x- and y-direction displacements for the measured points ($\times 10^{-4}$ m)							
Sam. No.	σ_{H} (MPa)	σ_{h} (MPa)	θ (°)		u_1	u_2	u_3	u_4	u_5	u_6	u_7
Training samples											
1	58.95	32.86	0	u_{x}	0.0019	−2.225	−4.43	−5.235	−4.513	−2.529	−0.4765
				u_y	0.6486	0.5579	0.2722	−0.2817	−0.6661	−0.9542	−1.247
2	56.86	48.12	0	u_{x}	−0.0073	−2.015	−3.894	−4.453	−3.773	−2.198	−0.2834
				u_y	2.638	2.205	1.307	−0.0042	−1.5940	−2.8940	−3.231
3	54.01	32.38	0	u_{x}	−0.0042	−2.046	−3.958	−4.655	−3.972	−2.248	−0.3338
				u_y	0.6566	0.5903	0.3139	−0.243	−0.6318	−0.9234	−1.21
4	48.51	43.22	0	u_x	−0.0071	−1.612	−3.069	−3.5	−2.974	−1.724	−0.1716
				u_y	2.284	1.891	1.129	−0.0036	−1.371	−2.283	−2.798
5	45.23	31.94	0	u_x	−0.0077	−1.61	−3.028	−3.524	−2.963	−1.685	−0.1719
				u_y	0.8638	0.7375	0.4316	−0.1669	−0.6455	−1.03	−1.309
6	42.04	31.14	0	u_x	−0.0076	−1.433	−2.673	−3.104	−2.614	−1.479	−0.1376
				u_y	0.8794	0.7372	0.4354	−0.1494	−0.6316	−1.023	−1.307
7	36.33	31.54	0	u_x	−0.0071	−1.091	−1.991	−2.288	−1.938	−1.086	−0.0072
				u_y	1.155	0.9359	0.5635	−0.0098	−0.7356	−1.233	−1.568
8	33.21	26.84	0	u_x	−0.0072	−0.985	−1.765	−2.047	−1.726	−0.9497	−0.0053
				u_y	0.6296	0.5024	0.3038	−0.1365	−0.4552	−0.7576	−1.008
9	30.41	21.86	0	u_x	−0.0032	−0.7596	−1.416	−1.728	−1.611	−0.816	−0.0047
				u_y	0.1765	0.1313	0.00619	−0.1965	−0.2839	−0.3745	−0.4811
10	59.42	33.12	20	u_x	1.417	−0.8006	−3.435	−4.961	−5.703	−4.107	−1.917
				u_y	0.8059	0.6107	0.4042	0.1395	−0.3262	−0.7111	−0.9687
11	57.06	48.32	20	u_x	1.221	−0.824	−3.116	−4.296	−4.679	−3.484	−1.659
				u_y	2.566	2.554	1.898	0.9066	−0.6904	−1.909	−2.787
12	53.96	32.37	20	u_x	1.26	−0.7932	−3.091	−4.384	−4.978	−3.6	−1.685
				u_y	0.7508	0.5941	0.4475	0.1687	−0.2879	−0.6621	−0.8762
13	50.26	31.28	20	u_x	1.122	−0.7402	−2.816	−3.973	−4.503	−3.26	−1.539
				u_y	0.7055	0.5601	0.4348	0.1645	−0.2612	−0.6115	−0.7955
14	48.44	42.52	20	u_x	0.9321	−0.6839	−2.497	−3.406	−3.711	−2.77	−1.32
				u_y	2.105	2.075	1.573	0.7407	−0.5675	−1.56	−2.267
15	42.02	30.52	20	u_x	0.7907	−0.6181	−2.183	−3.007	−3.342	−2.429	−1.141
				u_y	0.7971	0.6995	0.5673	0.2392	−0.2404	−0.637	−0.896
16	36.56	32.96	20	u_x	0.5516	−0.4964	−1.667	−2.218	−2.446	−1.806	−0.8353
				u_y	1.279	1.211	0.9673	0.4317	−0.3461	−0.9472	−1.387
17	32.48	26.56	20	u_x	0.4464	−0.4477	−1.441	−1.915	−2.146	−1.553	−0.706
				u_y	0.6012	0.4992	0.4483	0.1737	−0.1729	−0.465	−0.6737
18	30.88	22.56	20	u_x	0.4058	−0.3627	−1.244	−1.719	−2.122	−1.513	−0.6435
				u_y	0.2791	0.1065	0.1603	0.3489	−0.1361	−0.2601	−0.2844
19	57.92	44.12	40	u_x	3.008	0.6666	−1.439	−3.753	−4.723	−4.491	−3.05
				u_y	1.722	2.189	1.991	1.339	0.2946	−0.9394	−1.838
20	57.06	49.02	40	u_x	2.857	0.6309	−1.373	−3.554	−4.423	−4.19	−2.881
				u_y	2.235	2.839	2.628	1.767	0.4497	−1.177	−2.354
21	52.03	30.28	40	u_x	2.63	0.6564	−1.238	−3.365	−4.329	−4.332	−2.85
				u_y	0.5732	0.6652	0.5177	0.3599	−0.0655	−0.4077	−0.6647
22	49.61	40.52	40	u_x	2.37	0.5206	−1.175	−3.002	−3.75	−3.586	−2.436
				u_y	1.584	1.973	1.807	1.229	0.2724	−0.8324	−1.645
23	42.76	32.16	40	u_x	1.942	0.4258	−1.002	−2.526	−3.181	−3.078	−2.044
				u_y	0.826	0.9691	0.8538	0.6029	0.06014	−0.4314	−0.8326
24	38.14	28.97	40	u_x	1.583	0.3437	−0.8491	−2.107	−2.64	−2.574	−1.696
				u_y	0.7336	0.8398	0.7297	0.5242	0.03926	−0.3635	−0.7126

25	36.41	31.74	40	u_x	1.386	0.298	−0.7585	−1.86	−2.294	−2.238	−1.487
				u_y	1.066	1.271	1.138	0.7962	0.1385	−0.5171	−1.043
26	33.69	28.56	40	u_x	1.205	0.2569	−0.685	−1.656	−2.045	−2.012	−1.319
				u_y	0.8189	0.9445	0.8283	0.5918	0.07059	−0.3844	−0.7754
27	30.28	21.76	40	u_x	0.921	0.2193	−0.4973	−1.286	−1.66	−1.887	−1.17
				u_y	0.3789	0.2997	0.2037	0.1715	−0.1051	−0.1949	−0.2989
28	59.72	38.32	60	u_x	4.399	2.266	0.0186	−2.271	−4.483	−5.244	−4.411
				u_y	0.7726	1.261	1.251	1.052	0.5909	−0.2084	−0.9102
29	58.06	50.32	60	u_x	3.867	2.025	−0.0028	−2.004	−3.954	−4.535	−3.854
				u_y	1.563	2.615	2.891	2.393	1.414	−0.0309	−1.721
30	53.88	32.28	60	u_x	3.857	2.056	0.02733	−1.997	−3.937	−4.654	−3.983
				u_y	0.4741	0.8058	0.6517	0.5683	0.2956	−0.2501	−0.6245
Testing samples											
31	50.46	30.82	0	u_x	−0.0041	−1.859	−3.59	−4.228	−3.622	−2.043	−0.2594
				u_y	0.5807	0.5159	0.2726	−0.2344	−0.5692	−0.8246	−1.044
32	39.56	28.96	0	u_x	−0.0076	−1.324	−2.448	−2.848	−2.397	−1.346	−0.1173
				u_y	0.6752	0.5647	0.3338	−0.1582	−0.5147	−0.8318	−1.084
33	43.16	28.16	20	u_x	0.8633	−0.6086	−2.255	−3.159	−3.625	−2.617	−1.217
				u_y	0.5497	0.3961	0.3335	0.1088	−0.2033	−0.4723	−0.5936
34	34.48	22.56	20	u_x	0.5396	−0.3897	−1.454	−2.087	−2.684	−1.901	−0.807
				u_y	0.2517	0.4568	0.1073	−0.3137	−0.1838	−0.2797	−0.2399
35	54.06	32.57	40	u_x	2.828	0.674	−1.352	−3.583	−4.581	−4.484	−2.974
				u_y	0.7003	0.8348	0.6922	0.4841	−0.0159	−0.4628	−0.7966
36	32.15	25.43	40	u_x	1.121	0.2412	−0.6516	−1.57	−1.951	−1.939	−1.254
				u_y	0.5451	0.5857	0.485	0.3654	−0.0076	−0.2457	−0.4881
37	55.96	36.37	60	u_x	4.039	2.116	0.00085	−2.112	−4.129	−4.833	−4.066
				u_y	0.6905	1.128	1.08	0.9272	0.5255	−0.2026	−0.8146
38	37.56	29.96	60	u_x	2.069	1.131	−0.0051	−1.15	−2.178	−2.541	−2.153
				u_y	0.5484	0.8926	0.8907	0.7134	0.4253	−0.13	−0.6002
39	58.15	34.86	80	u_x	5.07	3.896	1.564	−0.6485	−3.227	−4.705	−5.344
				u_y	0.2506	0.6986	1.06	0.9069	0.6248	0.2583	−0.3158
40	38.54	26.96	80	u_x	2.694	2.044	0.8858	−0.3438	−1.722	−2.484	−2.903
				u_y	0.1473	0.4421	0.6457	0.5028	0.4042	0.1426	−0.1586

Tab.3: Earth stress magnitude and azimuth and corresponding displacements

of $T_w = 150\,^\circ$C, and the friction angle of fractures located in the mud-infiltrated region is reduced to 25 °C from 36 °C. The physical and mechanical properties of the intact rock and the properties of fracture are given in Table 1 [7]. Table 2 gives the mud and thermal properties. The blocks of intact rock are assumed to undergo elastoplastic deformation with the Drucker-Prager failure criterion and a non-associated flow rule. The deformation of the fractures is assumed to follow the Coulomb slip model.

In the 40 cases, a series of the different maximum and minimum horizontal earth stresses and azimuth are presented. The corresponding x- and y-direction displacement vectors in the given monitored points of the wellbore wall are calculated using UDEC model at $t = 60$ minutes. They all are shown in Table 3.

4.2. Verification

To verify the hybrid model established in this work, the training and testing samples in Table 3 are used to build the non-linear relationship between the earth stress magnitude

and direction and the borehole motions. And the necessary objective function is established based on the non-linear relationship.

In order to verify that the ANN(X) model can represent effectively the non-linear mapping between the earth stress magnitude and direction and the borehole motions. We put the entire data set through the network (training, validation and test), and analyze the network response (e.g., the mean square error and the ANN data regression).

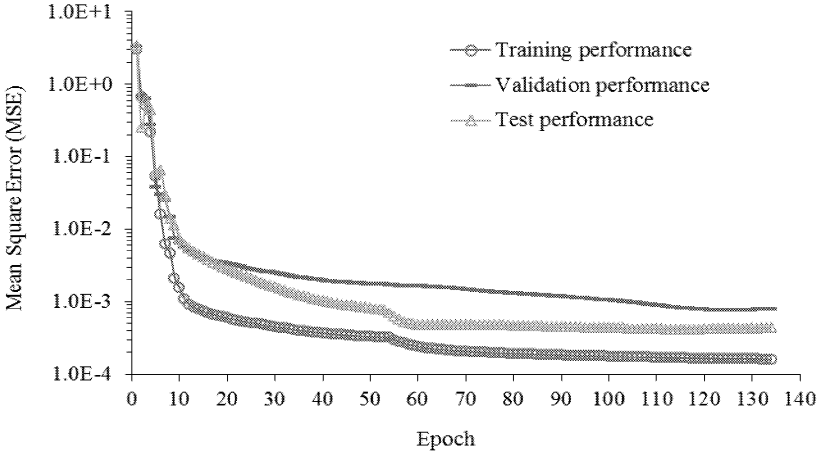

Fig.7: Variations of the mean square error

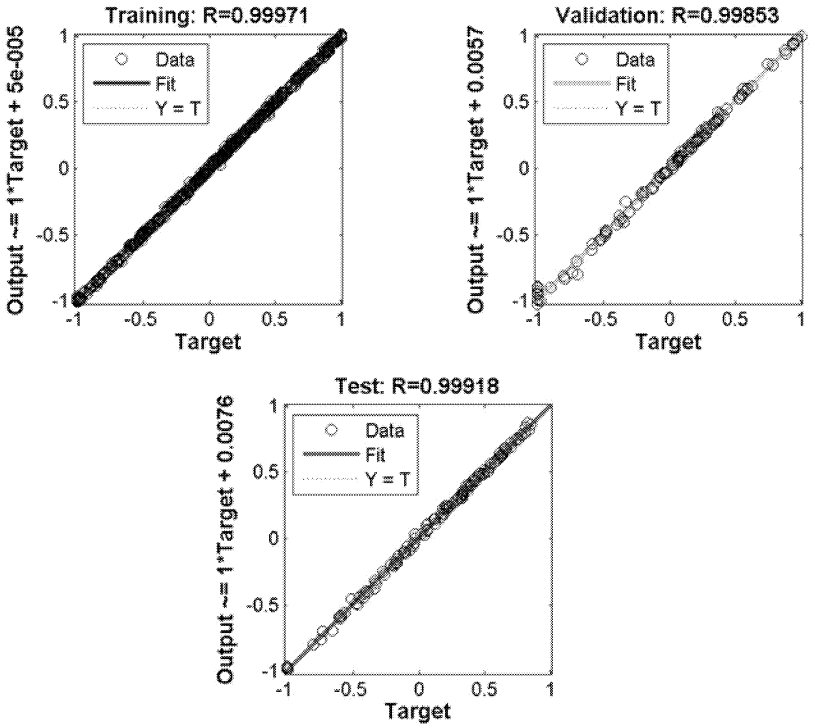

Fig.8: The linear regressions between the network outputs and the corresponding targets

As can be seen in Fig. 7, the training is stopped after 134 iterations because the validation error starts increasing. The final training set error value with a smaller mean-squared error is about 1.59×10^{-4}. The final validation set error and the final test set error with a smaller mean-squared error for both are about 7.8459×10^{-4} and 4.4159×10^{-4}, respectively. Results indicate that there is no significant overfitting occurring.

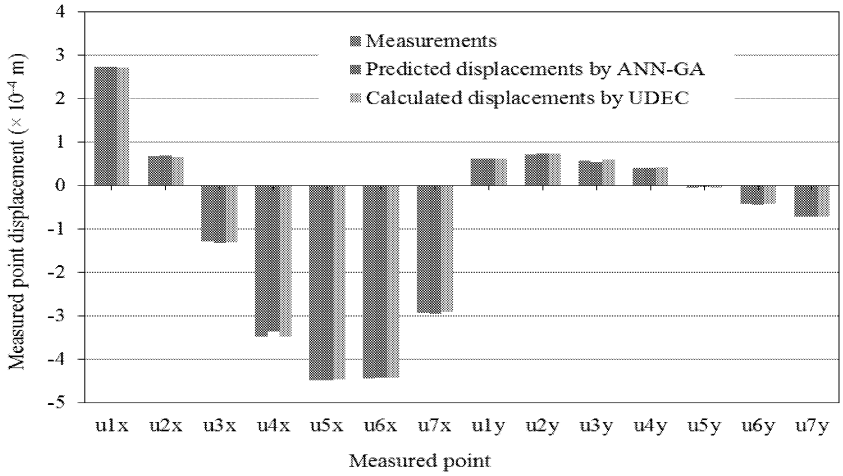

Fig.9: Comparison of displacements obtained by ANN-GA and displacements calculated through UDEC

	Displacements ($\times10^{-4}$ m)			Absolute error ($\times10^{-4}$ m)		Relative error	
	ANN-GA	UDEC	Measure-ment	ANN-GA and measurement	UDEC and measurement	ANN-GA and measurement	UDEC and measurement
u_{1x}	2.7351	2.726	2.727	0.0081	−0.001	0.00297	−0.000367
u_{2x}	0.694	0.6665	0.675	0.019	−0.0085	0.02815	−0.01259
u_{3x}	−1.329	−1.294	−1.291	−0.038	−0.003	0.02943	0.00232
u_{4x}	−3.3626	−3.473	−3.486	0.1234	0.013	−0.0354	−0.00373
u_{5x}	−4.4786	−4.453	−4.475	−0.0036	0.022	0.00080	−0.00492
u_{6x}	−4.4299	−4.412	−4.445	0.0151	0.033	−0.0034	−0.00742
u_{7x}	−2.958	−2.914	−2.932	−0.026	0.018	0.00887	−0.00614
u_{1y}	0.6267	0.6268	0.6141	0.0126	0.0127	0.02052	0.02068
u_{2y}	0.7316	0.7377	0.7227	0.0089	0.015	0.01231	0.02075
u_{3y}	0.5327	0.5927	0.5756	−0.0429	0.0171	−0.07453	0.02971
u_{4y}	0.4041	0.4134	0.4001	0.004	0.0133	0.00999	0.03324
u_{5y}	−0.04	−0.044	−0.05078	0.01078	0.00677	−0.2122	−0.13332
u_{6y}	−0.4469	−0.4305	−0.429	−0.0179	−0.0015	0.04172	0.0035
u_{7y}	−0.7132	−0.722	−0.7128	−0.0004	−0.0092	0.00056	0.01291

Tab.4: Comparison of predictions from ANN-GA model and calculations from UDEC model

	σ_H (MPa)	σ_h (MPa)	θ (°)
Searching range	[30, 60]	[20, 50]	[0, 90]
ANN-GA results	53.0516	31.2957	EN40.1786

Tab.5: Searching bound and identification results of parameters by the hybrid ANN-GA model

Fig. 8 shows the three linear regressions for training, validation and test between the network outputs and the corresponding targets. From Fig. 8 we can see that the three correlation coefficients (R-values) for training, validation and test are greater than 99 %. The scattered plots show a good correlation and regression values.

According to above analysis, ANN(X) model established in this work can accurately map the non-linear relationship between the earth stress magnitude and direction and the borehole motions, and provide the objective function for GA to search.

In this work, parameters of genetic algorithm are set as : maximum generation $N_{\max\_gen}$ = = 200, population size $N_{\text{pop\_size}} = 60$, crossover probability $P_c = 0.4$ and mutation probability $P_m = 0.2$. The ranges of parameters identified by ANN-GA are set as follows. The maximum horizontal earth stress, σ_H : 30.0–60.0 MPa, the minimum horizontal earth stress, σ_h : 20.0–50.0 MPa, the azimuth of the largest horizontal earth stress in east-north direction, θ : 0–90°.

Suppose the x- and y-direction displacements of the seven measured points (see Fig. 6) have been measured (as shown in Table 4). Based on the objective function, GA with the input of assumed measurements starts to search the optimal solution within the aforementioned ranges of the parameters to be recognized. After genetic operation of 200 generations of evolution, the final earth stress magnitude and direction obtained are given in Table 5 : The maximum horizontal earth stress, $\sigma_H = 53.0516$ MPa, the minimum horizontal earth stress, $\sigma_h = 31.2957$ MPa, the azimuth of the largest horizontal earth stress in east-north direction, $\theta = 40.1786°$.

Correspondingly, the ANN-GA model also gives the predicted x- and y-direction displacements at the seven measured points, which are shown in Table 4. In addition, Table 4 also gives the x- and y-direction displacements at the seven measured points, which are calculated by UDEC model.

For the displacement back analysis model, results of back-analysis can be assessed by the fitness with generations and the comparison among the predicted displacements and calculated displacements and the measured displacements. The predicted displacements by the hybrid ANN-GA and the calculated displacements by UDEC model at all seven measured points are compared with the measured displacements (as shown in Fig. 9 and Table 4). All absolute errors are less than 0.00002 m, and all relative errors are within 10 % except u_{5y}.

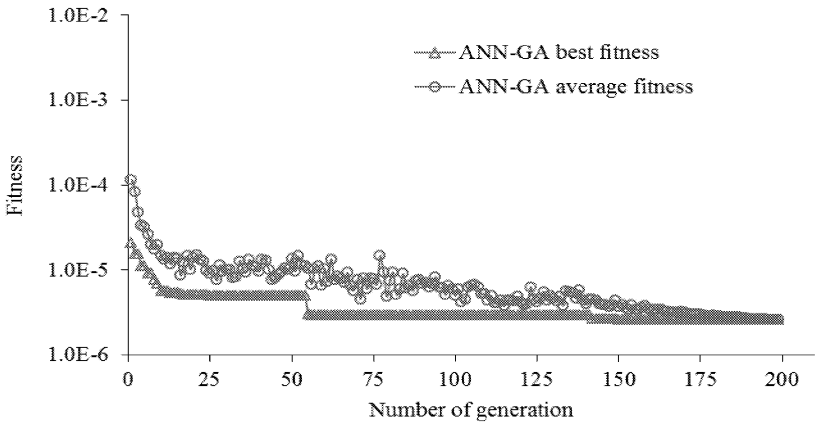

Fig.10: The variations of the fitness with generations

Fig. 10 shows the variations of the objective function values with generations. It can be seen from Fig. 10 that the final average individual fitness and the final best individual fitness are very close to the real value zero. They are 0.0261×10^{-4} and 0.0258×10^{-4} after genetic operation of 200 generations of evolution, respectively. Results demonstrate that the displacement back analysis method is effective for identification of the maximum and minimum horizontal earth stresses and the azimuth of the largest horizontal earth stress based on the borehole motions during drilling.

5. Conclusions

The displacement based inverse analysis presented in this paper is used for the identification of the earth stress based on the borehole motions during drilling. The method integrates genetic algorithm, artificial neural network and numerical analysis. In the numerical analysis, we used a coupled thermal-hydraulic-mechanical model in a thermoporoelsatoplasticity framework so that it would be possible to incorporate effects of mud, heat and plastic deformation taking place during drilling, to obtain borehole displacement vectors. In the displacement based inverse analysis, we use the hybrid ANN-GA model to identify the earth stress. The results of the mean-squared error and the linear regression for training, validation and test indicate that the ANN(X) model has a strong capability for self-learning and non-linear mapping between the earth stress and the borehole motions. Results of the fitness and the comparison between the predicted displacements and the measured displacements demonstrate clearly that the proposed method can accurately identify the earth stress based on the borehole motions induced by drilling.

References

[1] Aadnøy B.S.: Inversion technique to determine the earth stress field from fracturing data, J. Pet. Sci. Eng. 1990, 4, 127–141
[2] Aadnøy B.S.: In-situ stress directions from borehole fracture traces, J. Pet. Sci. Eng. 1990, 4, 143–153
[3] Aadnøy B.S., Belayneh M.: Elasto-plastic fracturing model for wellbore stability using non-penetrating fluids, J. Pet. Sci. Eng. 2004, 45, 179–192
[4] Aadnøy B.S., Bell J.S.: Classification of drilling-induced fractures and their relationship to earth stress directions, 1998,The Log Analyst 39(6), 27–42
[5] Abdallah G., Thoraval A., Steir A., Piguet J.P.: Thermal convection of fluid in fractured media, Int. J. Rock Mech. Min. Sci. & Geomech. Abstr. 1995, 32, 481–490
[6] Amadei B., Stephansson O.: Rock stress and its measurement, Chapman & Hall, 1997, London.
[7] Chen X., Tan C.P.: Detournay. A study on wellbore stability in fractured rock masses with impact of mud infiltration, J. Pet. Sci. Eng. 2003, 38, 145–154
[8] Christiansson R., Hudson J.A.: ISRM suggested methods for rock stress estimation – Part 4: Quality control of rock stress estimation, Int. J. Rock Mech. Min. Sci. 2003, 40, 1021–1025
[9] Cundall P.A., Hart R.D.: Numerical modeling of discontinue, Rngr. Comp. 1992, 9, 101–113
[10] Djurhuus J., Aadnøy B.S.: In situ stress state from inversion of fracturing data from oil wells and borehole image logs, J. Pet. Sci. Eng. 2003, 38, 121–130
[11] Fjær E., Holt R.M., Horsrud P., Raaen A.M., Risnes R.: Petroleum related rock mechanics, Second edition, 2008, UK
[12] Gjønnes M., Cruz A., Horsrud P., Holt R.M.: Leak-off tests for horizontal stress determination, J. Pet. Sci. Eng. 1998, 20, 63–71
[13] Haimson B.C., Cornet F.H.: ISRM suggested methods for rock stress estimation – Part 3: Hydraulic fracturing(HF) and/or hydraulic testing of pre-existing fractures (HTPF), Int. J. Rock Mech. Min. Sci. 2003, 40, 1011–1020

[14] Hareland G., Hoberock L.L.: Use of drilling parameters to predict in-site stress bounds, SPE 25727, In : Proc. 1993 SPE/IADC Drilling Conf., Amsterdam 1993, p. 457–171
[15] He L., An X.M., Ma G.W., Zhao Z.Y.: Development of three-dimensional numerical manifold method for jointed rock slope stability analysis, Int. J. Rock Mech. Min. Sci. 2013, 64, 22–35
[16] Hilchie D.W.: Caliper logging – Theory and practice, The log Analyst 1968, IX, 3–12
[17] Holland J.H.: Adaptation in natural and artificial systems, Ann Arbor, MI, University of Michigan Press, 1975
[18] Hudson J.A., Cornet F.H., Christiansson R.: ISRM suggested methods for rock stress estimation – Part 1 : Strategy for rock stress estimation, Int. J. Rock Mech. Min. Sci. 2003, 40, 991–998
[19] Itasca. UDEC user's manual, Itasca Consulting Group, Minneapolis, MM, USA, 2011
[20] Lewis R.W., Schrefler B.A.: The finite element method in the static and dynamic deformation and consolidation of porous media, John Wiley and Sons, 1998, New York
[21] Ljunggren C., Chang Y., Janson T., Christiansson R.: An overview of rock stress measurement methods, Int. J. Rock Mech. Min. Sci. 2003, 40, 975–989
[22] Maranuk C.: Development of an MWD hole caliper for drilling and formation evaluation, SPE Annual Technical Conference and Exhibition, San Antonio, Texas 1997
[23] McCulloch W.S., Pitts W.H.: A logical calculus of the ideas immanent in nervous activity, Bull Math. Biophys. 1943, 5, 115–133
[24] Nicolson J.P.W., Hunt S.P.: Distinct element analysis of borehole instability in fractured petroleum reservoir seal formation, SPE Asia and Pacific Oil and Gas Conference and Exhibition, SPE 88610, Perth, Australia, 2004, p. 1–4
[25] Nikravesh M., Aminzadeh F. Zadeh L.A.: Soft computing and intelligent data analysis in oil exploration, Elsevier Science B.V. 2003, Boston
[26] Okabe T., Hayashi K., Shinohara N. and Takasugi S.: Inversion of Drilling-induced Tensile Fracture Data obtained from a Single inclined Borehole, Int. J. Rock Mech. Min. Sci. 1998, 35, 747–758
[27] Pinzon J.A., Dowla N., Real-Time Wellbore-Quality Evaluation for Drilling Optimization, ACIPETX Congreso Colombiano del Petróleo, Bogotá D.C., Colombia, 2003
[28] Prochazka P.P.: Rock bursts due to gas explosion in deep mines based on hexagonal and boundary elements, Adv. Eng. Software, 2013
[29] Rabczuk T., Belytschko T. , Xiao S.P.: Stable particle methods based on Lagrangian kernels , Comput. Methods Appl. Mech. Engrg. 2004, 193, 1035–1063
[30] Sahoo G.B., Ray C.: Flow forecasting for a Hawaiian stream using rating curves and neural networks, J. Hydrol. 2006, 317, 63–80
[31] Sjöberg J., Christiansson R., Hudson J.A.: ISRM suggested methods for rock stress estimation – Part 2 : Overcoring methods, Int. J. Rock Mech. Min. Sci. 2003, 40, 999–1010
[32] Zemanek J., Glenn E.E., Norton L.J., Cardwell R.L.: Formation evaluation by inspection with the borehole televiewer, Geophysics 1970, 35, 254–269
[33] Zhang S., Yin S.: Determination of horizontal in-situ stresses and natural fracture properties from wellbore deformation. International Journal of Oil, Gas and Coal Technology, 2014, 7, 1–28
[34] Zhang S., Yin S.: Reservoir geomechanical parameters identification based on ground surface movements, Acta Geotech. 2013, 8(3), 279–292
[35] Zhang S., Yin S., Yuan Y.: Estimation of fracture stiffness, in-situ stresses and elastic parameters of naturally fractured geothermal reservoirs. International Journal of Geomechanics, doi : 10.1061/(ASCE)GM.1943-5622.0000380, 2013
[36] Zhang, S.: Petroleum geomechanics characterization using coupled numerical modeling and soft computing, University of Wyoming, Ph.D thesis 2013

Received in editor's office: September 12, 2013
Approved for publishing: March 7, 2014